

**Structure, Volume 32**

**Supplemental Information**

**Dissecting the molecular basis for the modulation  
of neurotransmitter GPCR signaling by GINIP**

**Alex Luebbbers, Alberto J. Gonzalez-Hernandez, Myles Zhou, Stephen J. Eyles, Joshua Levitz, and Mikel Garcia-Marcos**

# FIGURE S1

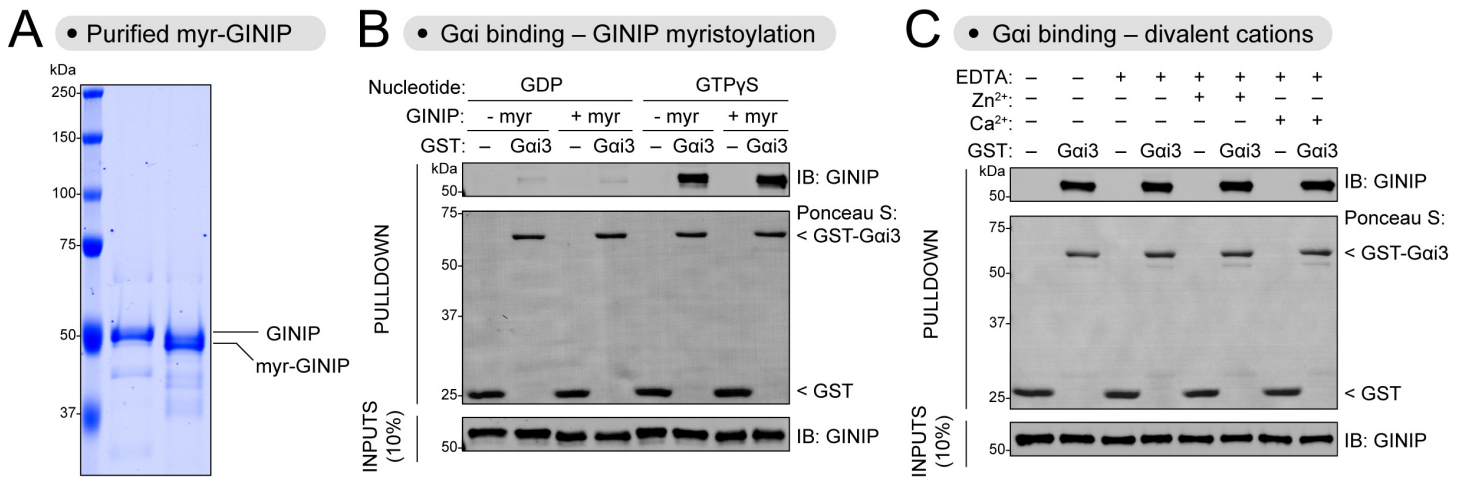


**Figure S1. Neither GINIP myristoylation nor presence of divalent cations affects binding to Gai3. Related to Figure 1.**

**(A)** His-tagged non-myristoylated and myristoylated-GINIP (myr-GINIP) purified from bacteria were run in an 8% SDS-PAGE gel supplemented with 4M urea before Coomassie staining. Two  $\mu\text{g}$  of each protein were loaded. Myr-GINIP displays a downward shift compared to GINIP.

**(B)** Myristoylation of GINIP does not affect binding to Gai3. Purified GINIP or myr-GINIP were incubated with GST or GST-Gai3 immobilized on glutathione-agarose beads in the presence of GDP or GTP $\gamma$ S as indicated. Bead-bound proteins were detected by Ponceau S staining or by immunoblotting (IB) as indicated.

**(C)** Divalent cations do not affect the binding of GINIP to Gai3. Purified GINIP was incubated with GST or GST-Gai3 immobilized on glutathione-agarose beads in buffers with the indicated additives (Zn<sup>2+</sup> = ZnCl<sub>2</sub>, Ca<sup>2+</sup> = CaCl<sub>2</sub>). All conditions contained GTP $\gamma$ S. Bead-bound proteins were detected by Ponceau S staining or by immunoblotting (IB).

Results are representative of  $n \geq 3$  experiments.

# FIGURE S2

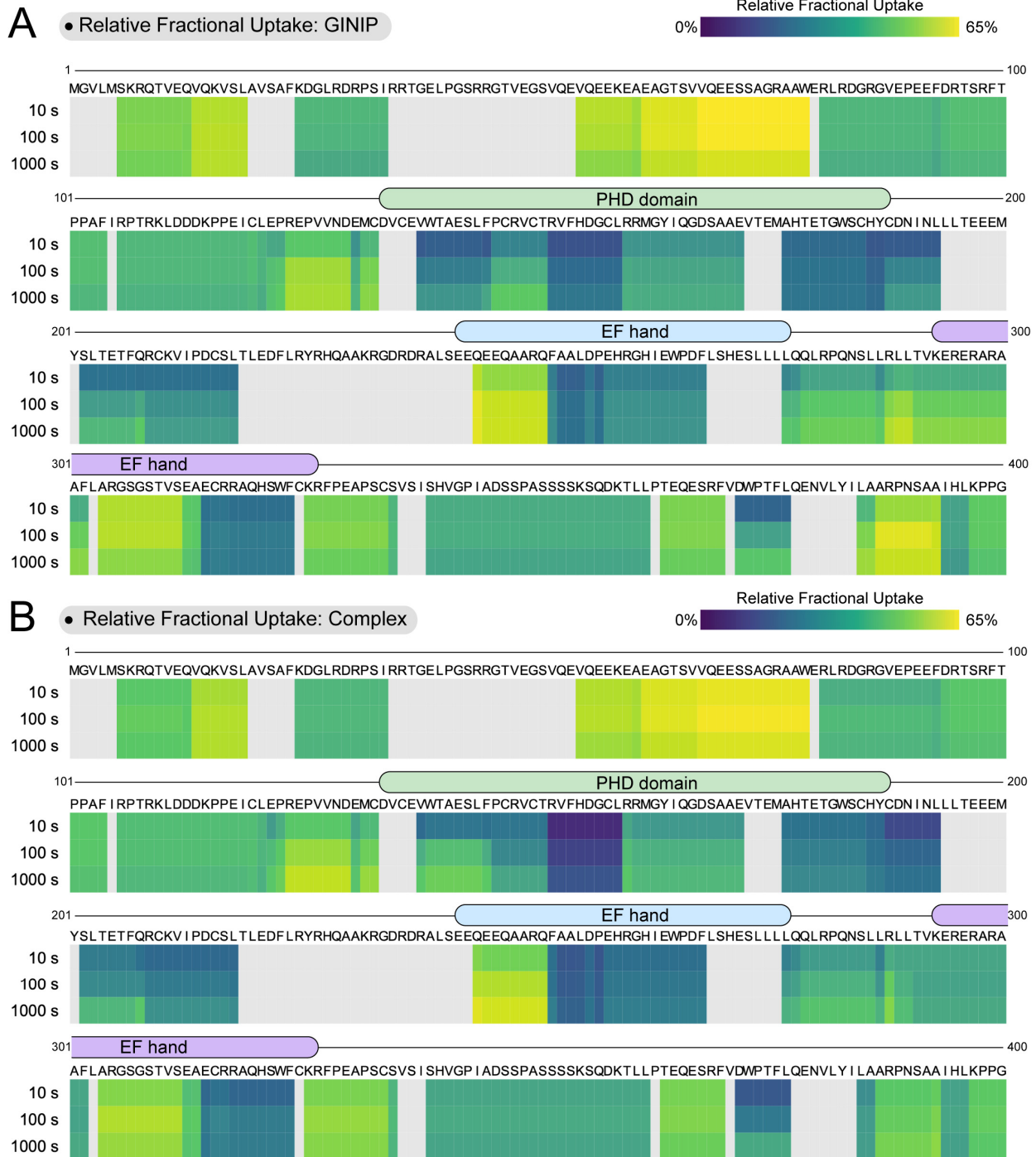


**Figure S2. Relative fractional uptake of GINIP alone or in complex with Gai3. Related Figure 2.**

**(A, B)** Stacked heat maps showing relative fractional uptake of deuterium by GINIP peptides from GINIP alone (A) or the GINIP:Gai complex (B) at different times (10 s, 100 s, 1000 s), where navy blue is no exchange and yellow is maximal exchange measured. Grey indicates regions without peptide coverage. Data are the mean relative fractional uptake of an experiment run in quadruplicates.



uptake (Region 4 and 5). This heat map is reproduced from **Fig 2. Top & Bottom**, mutation of indicated single residues in Regions 1, 2, 4, and 5 did not reduce binding for those mutants that were expressed. Lysates of HEK293T cells expressing the indicated GINIP mutants were incubated with GST or GST-Gai3 immobilized on glutathione-agarose beads in the presence of GDP, GDP·AlF<sub>4</sub><sup>-</sup>, or GTPγS, as indicated. Bead-bound proteins were detected by Ponceau S or by immunoblotting (IB).

All protein electrophoresis results are representative of  $n \geq 3$  experiments.

## FIGURE S4

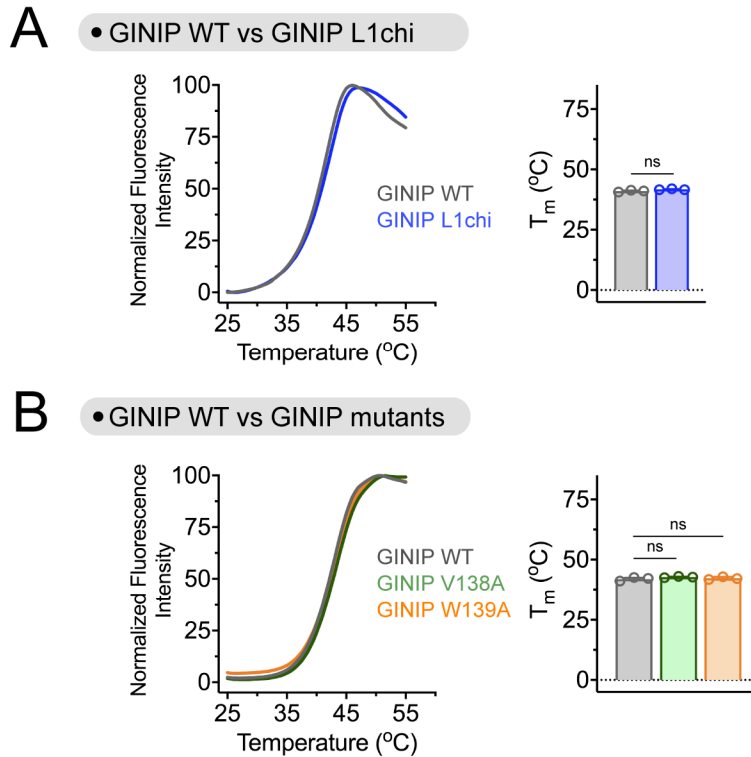


**Figure S4. GINIP mutant proteins display the same thermal stability as GINIP WT. Related to Figure 3 and 4.**

**(A, B)** GINIP L1chi, GINIP V138A, and GINIP W139A have thermal stability similar to GINIP WT as measured by Differential Scanning Fluorimetry (DSF). *Left graphs*, Thermal denaturation curves comparing GINIP L1chi (blue, A) or GINIP V138A (green, B) and W139A (orange, B) to GINIP WT (grey, A and B). SYPRO Orange Fluorescence was measured to track denaturation as temperature of protein samples was increased over time. Mean,  $n=3$ . *Right graphs*, Quantified melting temperature ( $T_m$ ) of GINIP mutants compared to GINIP WT based on the sigmoid of the denaturation curves. Mean  $\pm$  S.E.M.,  $n=3$ , ns = not significant for t-test in A and one-way ANOVA corrected for multiple comparisons (Tukey) in B.

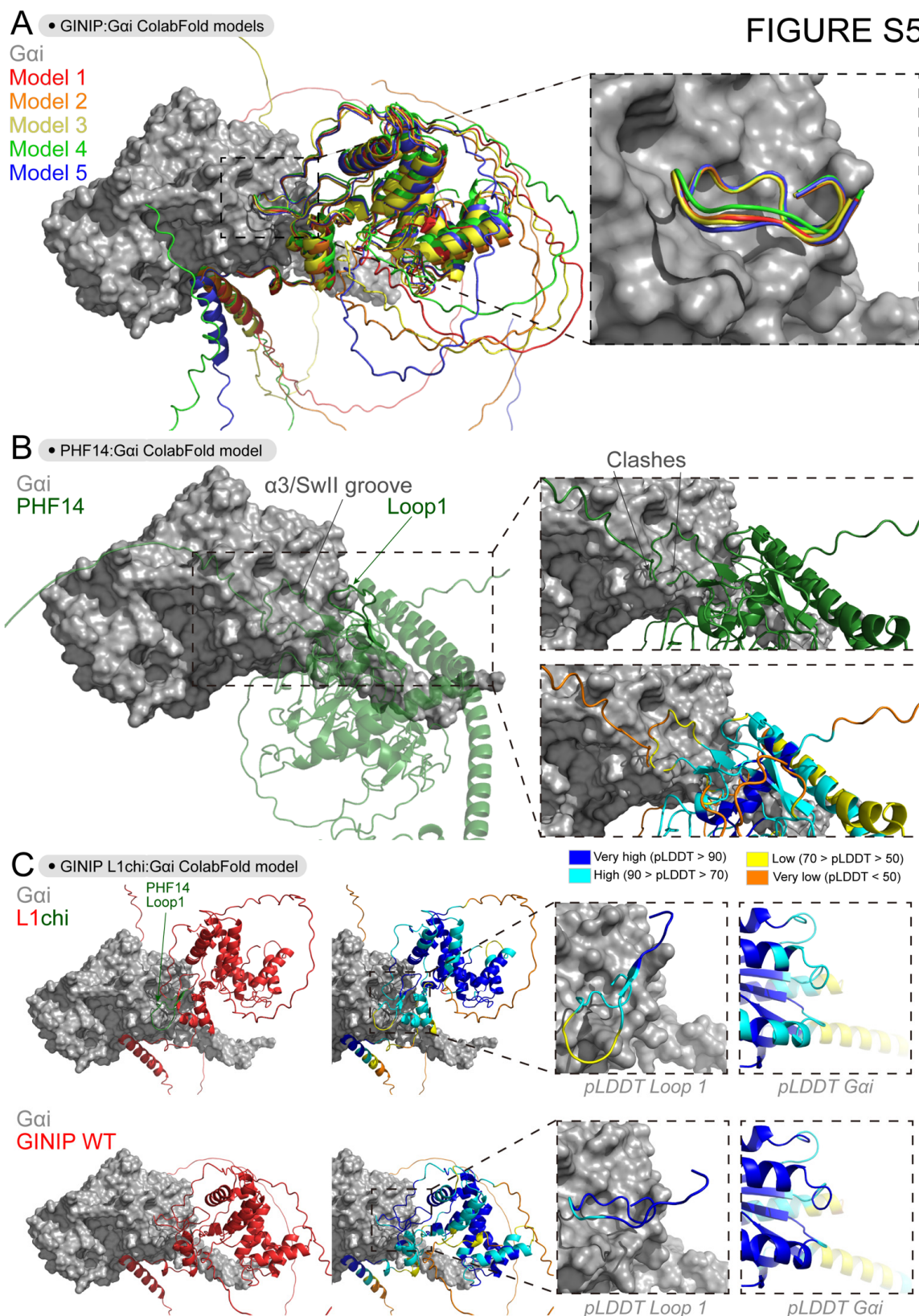


**Figure S5. Comparison of ColabFold models of Gai in complex with GINIP WT, PHF14, or GINIP L1chi. Related to Figure 5.**

**(A)** Multiple GINIP:Gai ColabFold models show similar predictions for the docking of Loop 1 of the PHD domain of GINIP onto the  $\alpha$ 3/SwII groove of Gai. *Left*, protein folding model of GINIP (overlaid colors) bound to Gai (grey) was generated using ColabFold. Models are ranked 1 to 5 from high to low confidence. *Right*, image

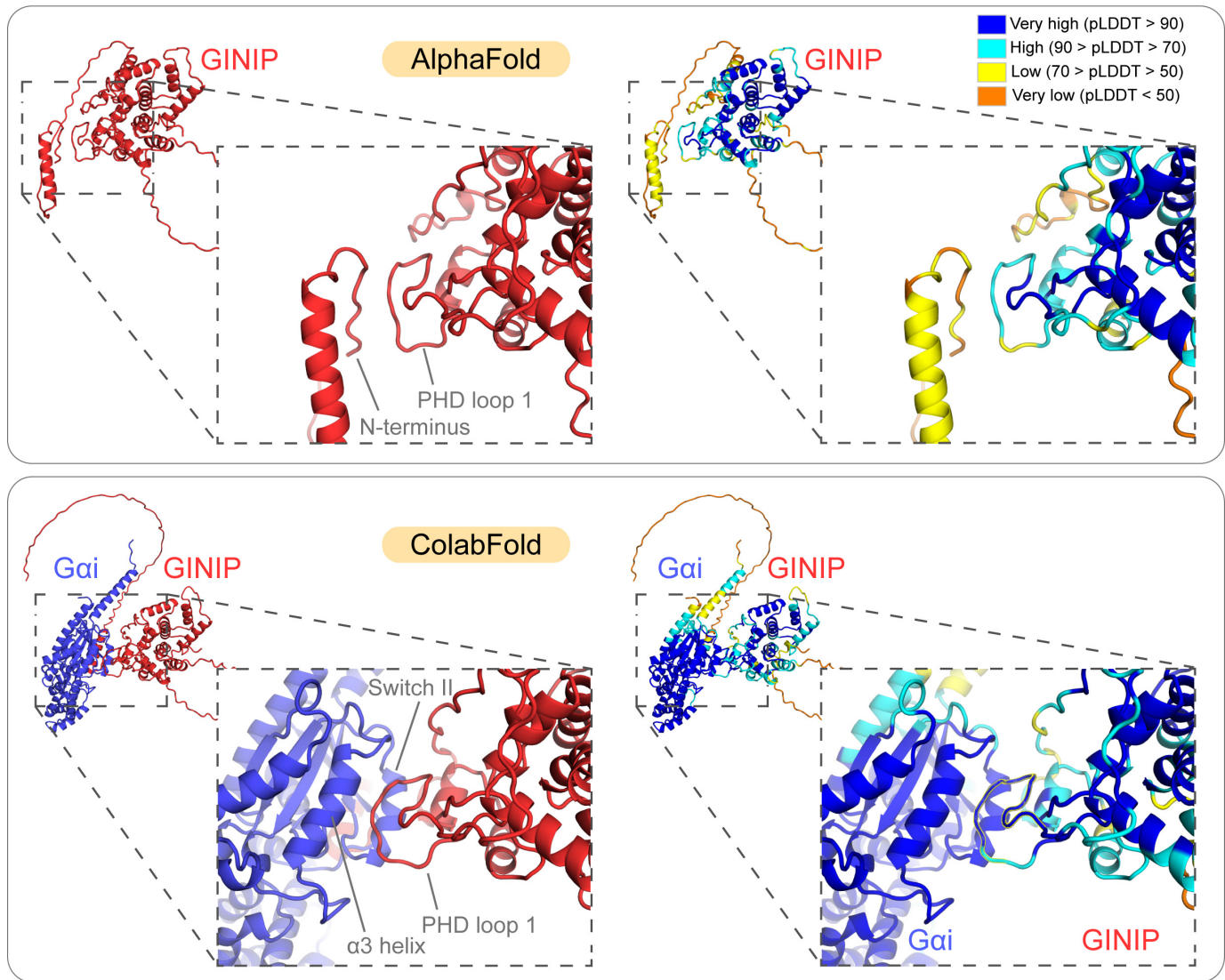
showing a closeup of the Loop 1 of the PHD domain of GINIP from the different models (multiple colors) fitting into the  $\alpha$ 3/SwII groove of Gai (grey).

**(B)** A PHF14:Gai ColabFold model shows a poor fit for the interaction and intermolecular clashes. *Left*, protein folding model for the complex of PHF14 (green) bound to Gai (grey) was generated using ColabFold. *Right*, images of a closeup of the predicted PHF14:Gai showing clashes and low pLDDT values.

**(C)** A GINIP L1Chi:Gai ColabFold model shows a poor fit between the Loop1 of the PHD domain of the chimera and Gai compared to GINIP WT. Protein folding models for the complex of GINIP L1chi (*top row*: GINIP, red; PHF14 Loop 1, green) or GINIP WT (*bottom row*: GINIP, red) bound to Gai (grey) show a similar overall pose, but the Loop1 engages more superficially and the pLDDT values at the predicted protein interface are lower for the complex with the chimera compared to GINIP WT.

**A** • GINIP and GINIP:Gai folding models

**FIGURE S6**



**B** • GINIP N-terminal truncations

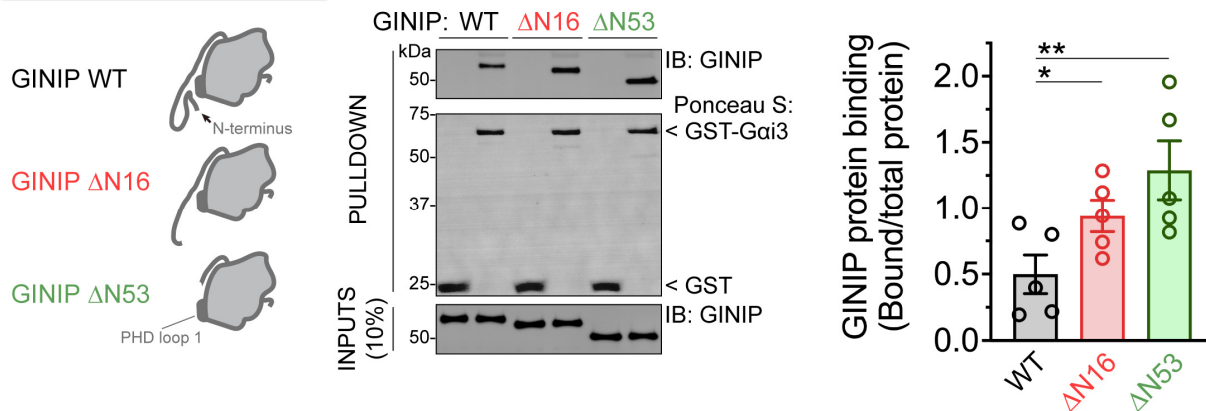


**Figure S6. Putative intramolecular contact between the N-terminus of GINIP and the Loop 1 of the PHD domain. Related to Figure 6.**

**(A)** The N-terminus of GINIP might be in the vicinity of the Loop 1 of the PHD domain in the absence of Gai but not when bound to the G protein. The AlphaFold 2.0 model of GINIP alone is shown on the top, and the ColabFold model of GINIP in complex with Gai is shown on the bottom. GINIP and Gai are colored red and blue, respectively

on the left, whereas the panels on the right are colored based on predicted local difference test (pLDDT) scores, a per-residue confidence metric measured on a scale of 0-100.

**(B)** N-terminally truncated GINIP constructs display modest increases in binding to Gai3. *Left*, schematic representation of N-terminal truncations of GINIP removing residues 1-16 ( $\Delta$ N16) or 1-53 ( $\Delta$ N53) and the resulting exposure of the PHD Loop 1 G protein binding site. *Center*, Purified His-tagged GINIP WT, GINIP  $\Delta$ N16, or GINIP  $\Delta$ N53 were incubated with GST or GST-Gai3 immobilized on glutathione-agarose beads in the presence of GTP $\gamma$ S. Bead-bound proteins were detected by Ponceau S staining or by immunoblotting (IB). A representative experiment of n=5 is shown on the left, and a graph with the quantification of binding is shown on the right. Mean  $\pm$  S.E.M., \*p<0.05, \*\*p<0.01, paired one-way ANOVA corrected for multiple comparisons (Tukey).

# FIGURE S7

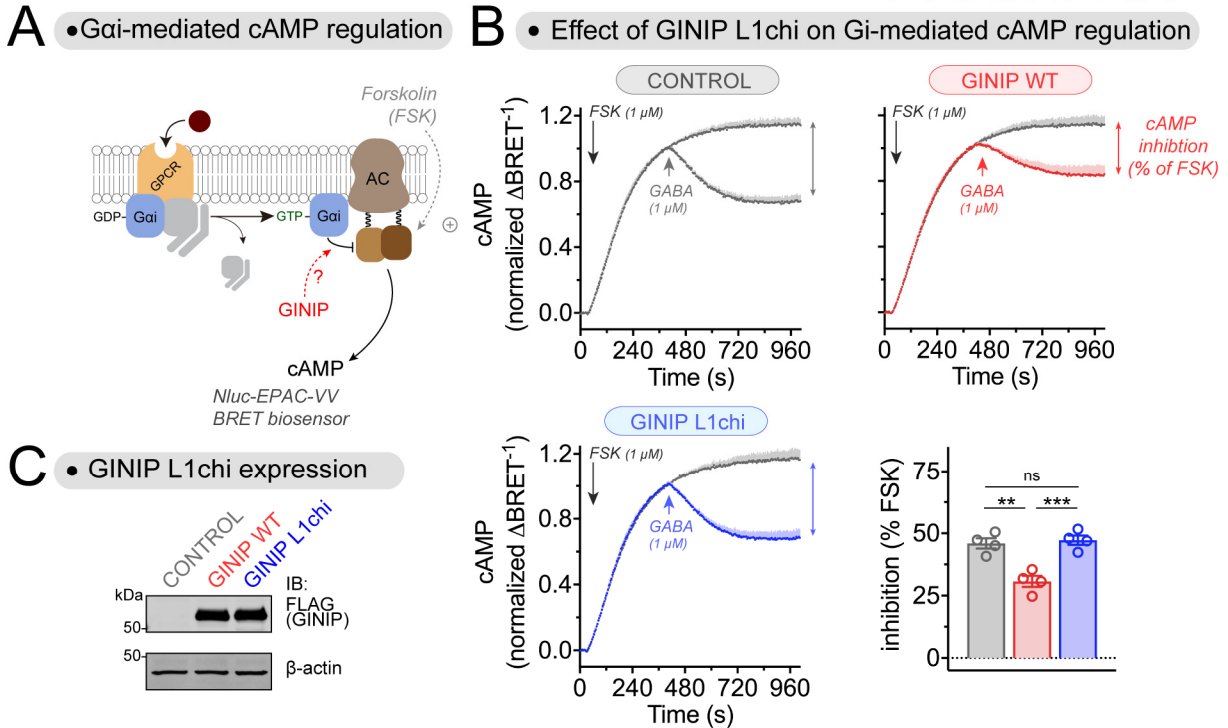


**Figure S7. GINIP L1chi fails to regulate cAMP cellular levels upon GPCR stimulation. Related to Figure 7.**

**(A)** Diagram of GPCR-mediated activation of Gai-GTP and subsequent regulation of cAMP levels in cells monitored by BRET.

**(B)** Replacement of the Loop 1 of the PHD domain in the GINIP L1chi construct prevents the blockade of cAMP inhibition upon stimulation of GABA<sub>B</sub>R observed with GINIP WT. Kinetic BRET measurements of cAMP levels were carried out in HEK293T cells expressing the GABA<sub>B</sub>R without GINIP (gray) or expressing GINIP WT (red) or GINIP L1chi (blue). Cells were treated with forskolin (FSK) and GABA as indicated. Quantification of the inhibition of FSK-stimulated cAMP upon stimulation of GABA<sub>B</sub>R with GABA is shown in the bar graph on the bottom left corner. Mean  $\pm$  S.E.M.,  $n=4$ . ns = not significant, \*\* $p<0.01$ , \*\*\* $p<0.001$ , one-way ANOVA corrected for multiple comparisons (Tukey).

**(C)** Representative immunoblotting (IB) result confirming equal expression of GINIP WT and GINIP L1chi in the cells used for the experiments shown in (B).

# FIGURE S8

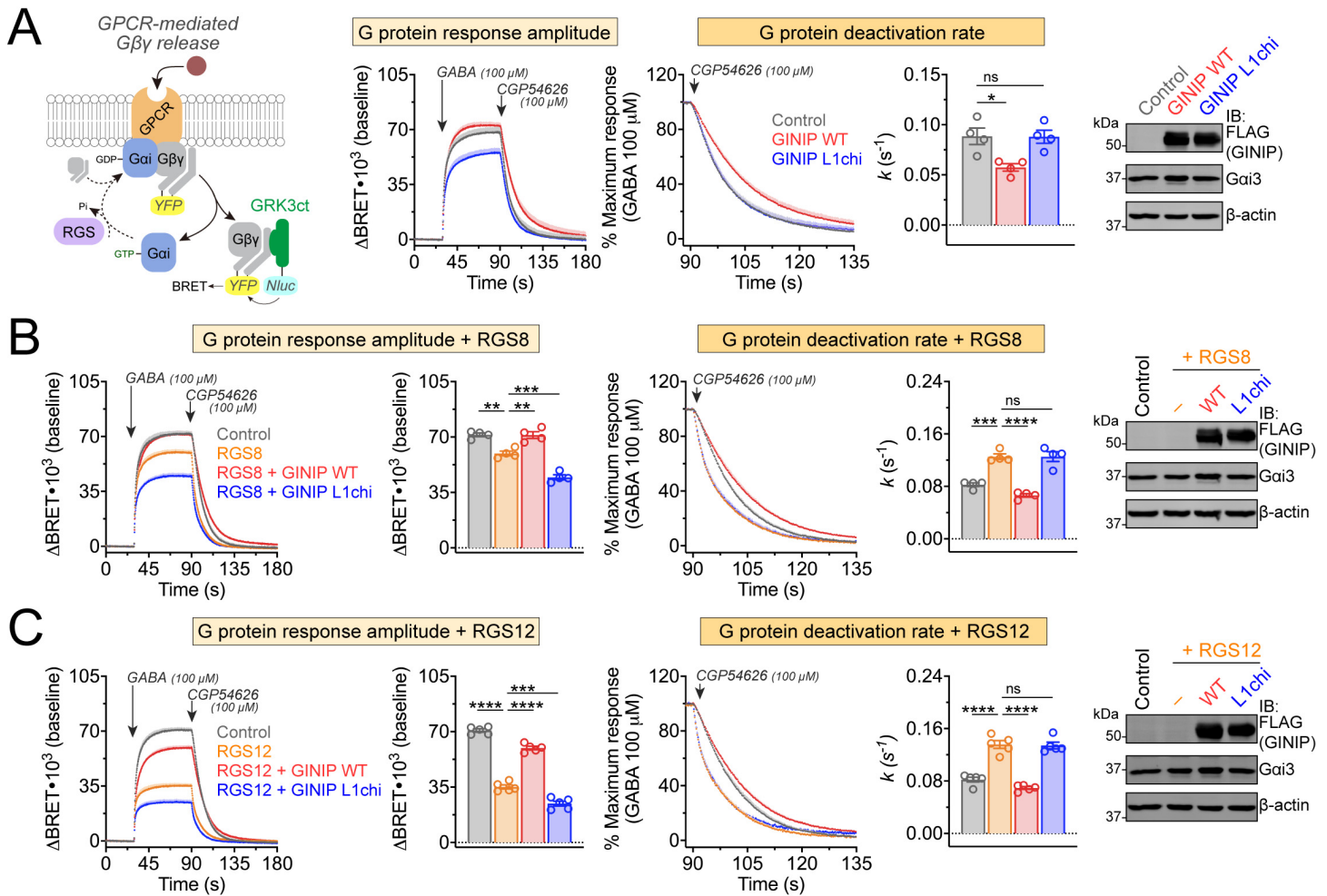


**Figure S8. GINIP L1chi fails to regulate Gβγ responses in cells upon GPCR stimulation. Related to Figure 8.**

**(A)** Expression of GINIP Loop 1 chimera (L1chi) prevents the enhancement of Gβγ signaling upon stimulation of GABA<sub>B</sub>R observed with GINIP WT. *Left*, diagram of G protein activation/deactivation cycle and BRET-based detection of free Gβγ. *Center*, kinetic BRET measurements were carried out in HEK293T cells expressing the GABA<sub>B</sub>R without GINIP (grey), or expressing GINIP WT (red) or GINIPL1chi (blue). Cells were treated with GABA and CGP54626 as indicated. *Right*, G protein deactivation rates were determined by normalizing the BRET data to maximum response and fitting the post-antagonist data to an exponential decay curve to extract rate constant values ( $k$ ). Mean  $\pm$  S.E.M.,  $n=4$ . ns = not significant,  $*p<0.05$ , one-way ANOVA corrected for multiple comparisons (Tukey). A representative immunoblotting (IB) result confirming equal expression of GINIP WT, GINIPL1chi, and Gai3 in these experiments is shown on the right.

**(B)** Replacement of Loop 1 of GINIP ablates RGS8-mediated regulation of Gβγ signaling upon stimulation of GABA<sub>B</sub>R observed with GINIP WT. BRET experiments were carried out and analyzed as in (A) with cells expressing RGS8 alone (orange), RGS plus GINIP WT (red), RGS plus GINIPL1chi (blue), or neither RGS8 nor GINIP (grey). Quantification of G protein response amplitude was determined 1 minute after agonist stimulation. Mean  $\pm$  S.E.M.,  $n=4$ . ns = not significant,  $**p<0.01$ ,  $***p<0.001$ ,  $****p<0.0001$ , one-way ANOVA corrected for multiple comparisons (Tukey).

**(C)** Replacement of Loop 1 of GINIP ablates RGS12-mediated regulation of G $\beta\gamma$  signaling upon stimulation of GABA<sub>B</sub>R observed with GINIP WT. BRET experiments were carried out and analyzed as in (A) with cells expressing RGS12 alone (orange), RGS plus GINIP WT (red), RGS plus GINIPL1chi (blue), or neither RGS8 nor GINIP (grey). Quantification of G protein response amplitude was determined 1 minute after agonist stimulation. Mean  $\pm$  S.E.M., n=5. ns = not significant, \*\*\*p<0.001, \*\*\*\*p<0.0001, one-way ANOVA corrected for multiple comparisons (Tukey). A representative immunoblotting (IB) result confirming equal expression of GINIP WT, GINIP mutants, and Gai3 in these experiments is shown on the right.